ACS APPLIED MATERIALS & INTERFACES

Research Article

www.acsami.org

Planar Porous Graphene Woven Fabric/Epoxy Composites with Exceptional Electrical, Mechanical Properties, and Fracture Toughness

Xu Liu, Xinying Sun, Zhenyu Wang, Xi Shen, Ying Wu, and Jang-Kyo Kim*

Department of Mechanical and Aerospace Engineering, The Hong Kong University of Science and Technology, Clear Water Bay, Kowloon, Hong Kong

Supporting Information

ABSTRACT: Planar interconnected graphene woven fabrics (GWFs) are prepared by template-based chemical vapor deposition and the GWFs are employed as multifunctional filler for epoxy-based composites. Apart from flexibility, transparency, lightweight, and high electrical conductivity, the GWFs have unique morphological features consisting of orthogonally interweaved, inherently percolated, hollow graphene tubes (GTs). The orthogonal GT structure means that the GWF/epoxy composites hold significant anisotropy in mechanical and fracture properties. The composites with 0.62 wt % graphene deliver a combination of excellent electrical and fracture properties: e.g., an electrical conductivity of ~0.18 S/cm; and fracture toughness of 1.67 and 1.78 MPa·m$^{1/2}$ when loaded along the 0° and 45° directions relative to the GT direction, respectively, equivalent to notable 57% and 67% rises compared to the solid epoxy. Unique fracture processes in GWF/epoxy composites are identified by in situ examinations, revealing crack tip blunting that occurs when the crack impinges GTs, especially those at 45° to the crack growth direction, as well as longitudinal tearing of hollow GTs as the two major toughening mechanisms.

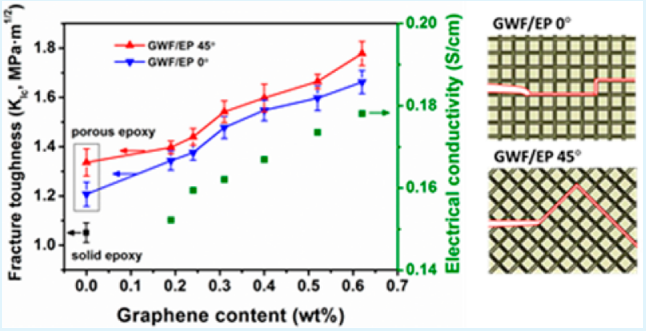

KEYWORDS: *graphene woven fabric, orthogonal graphene tubes, porous structure, fracture toughness, anisotropic properties*

1. INTRODUCTION

Graphene, a two-dimensional, hexagonal monolayer of carbon atoms, has been widely studied due to its unique structure, extremely large surface area, remarkable electrical, mechanical and thermal properties.[1−5] To harness these excellent properties, graphene or graphene oxide (GO) sheets are often incorporated into a polymer matrix to form graphene-based nanocomposites[6,7] which can offer multifunctional characteristics,[8] like electromagnetic interference (EMI) shielding,[9] energy storage,[10,11] thermal management applications,[12−15] and various sensing capabilities.[16−18] However, previous studies have shown that the enhancements of the properties of graphene/polymer composites prepared by simply mixing reduced GO (rGO) or graphene nanoplates (GNPs) with a polymer matrix were not as substantial as expected. There are many important challenges that must be overcome for graphene-based composites to achieve their full potentials, such as the synthesis of high quality graphene or GO,[19] uniform dispersion,[20−22] alignment of graphene,[23,24] and reduction of GO.[25]

In addition to 2D graphene or GO sheets, rationally assembled graphene structures have been recognized as another fascinating means of imparting graphene's unique characteristics to composites. Three-dimensional (3D) graphene structures, like graphene aerogels (GAs),[26−28] graphene foams (GFs),[29−32] and graphene woven fabrics (GWFs),[33,34] possessing interconnected networks with very large surface areas and high porosities, have opened opportunities in fabricating a new class of composites with multifunctional capabilities that 2D graphene cannot provide. The GFs or GAs can eliminate the issue of agglomeration of graphene in a polymer matrix while offering a cellular architecture with inherently interconnected conductive networks, so as to significantly improve the electrical properties of the composites. Besides, the GFs and GWFs synthesized by a chemical vapor deposition (CVD) method have captured tremendous attention as promising filler materials for composites. Compared to graphene or GO sheets prepared by chemical or mechanical exfoliation of natural graphite, graphene prepared by the template-based CVD technique exhibits multitudinous advantages, including high-quality sp^2 structure with virtually no defects and continuous graphene architecture with desired configurations.[35]

Received: July 17, 2015
Accepted: September 2, 2015
Published: September 2, 2015

DOI: 10.1021/acsami.5b06476
ACS Appl. Mater. Interfaces 2015, 7, 21455−21464

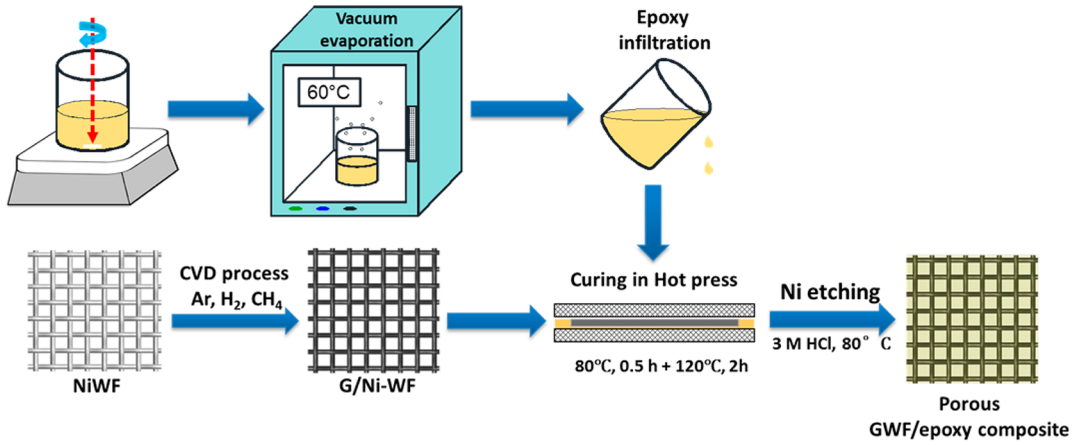

Figure 1. Schematic flowchart of the fabrication processes of GWF/epoxy composites.

GF/polydimethylsiloxane (PDMS) composites[29] were fabricated by CVD growth graphene on Ni foam and simple coating of GFs with PDMS. The flexible, porous composites showed outstanding electrical properties, and a high specific EMI shielding efficiency of about 500 dBcm^3/g with a graphene content less than 0.8 wt %. The cellular-structured GF/epoxy composites[32] also displayed a remarkable electrical conductivity of 3 S/cm at 0.2 wt % graphene, and the corresponding flexural modulus and strength increased by 53% and 38% respectively, compared to the neat epoxy. Apart from the porous structure in GFs, GWFs grown on Ni or Cu woven fabric templates also have a rationally designed architecture in which hollow graphene tubes (GTs) are cross-linked orthogonally in the plane direction. The GWFs synthesized using CH_4 flows in a CVD process[33] have shown an excellent electromechanical response in PDMS-based composite films and a high potential for photovoltaic applications together with conducting polymers. The GWF/PDMS system can serve as strain sensors[34,36] due to the unique crack formation and propagation mechanism of GWFs with a low electrical resistance, as well as the flexible PDMS matrix that can undergo a large elastic deformation. The core/shell multilayer GWF/porous carbon hybrid structures[37] and GWFs held by a cloth[38] also displayed excellent electromechanical characteristics when used as supercapacitor electrodes.

In this study, we report the fabrication of GWFs on Ni woven fabrics and composites by infiltrating epoxy into the graphene/Ni woven fabrics. The GWF/epoxy composites have orthogonally interconnected GT networks after removing the Ni templates. The composites presented excellent electrical, mechanical properties, and fracture toughness. They exhibited unique toughening mechanisms that have never been reported for other graphene-based composites.

2. EXPERIMENTAL SECTION

2.1. Synthesis of GWFs. Ni woven fabric templates (supplied by Beijing Century Woven Corp.) were cleaned with diluted HCl, acetone, and deionized (DI) water in sequence by ultrasonication. After drying in a vacuum oven for 24 h, the Ni templates were cut into pieces into 10 cm × 5 cm rectangles and placed into the quartz tube of the CVD furnace (OTF-1200X-II-80-SL, Hefei Kejing Materials). The furnace was heated from room temperature to 1000 °C at a ramp rate of 17 °C/min and the Ni surface was annealed under Ar (200 standard cubic centimeter per minute (sccm)) and H_2 (100 sccm) flows for 1 h. CH_4 was subsequently introduced into the furnace for deposition of graphene for 20 min. The furnace was rapidly cooled to ambient temperature under Ar and H_2 flows, and graphene layers were formed on the template surface. The as-prepared graphene/Ni woven fabrics were used to prepare composites. Freestanding GWFs were obtained after etching the Ni templates by immersion in a 0.5 M $FeCl_3$/1 M HCl mixture at 80 °C for 2 h. Polyethylene terephthalate (PET) thin films were used to collect the freestanding GWFs from the solution. GWFs consisting of different numbers of graphene layers were prepared by varying the CH_4 feed rates from 0.5 to 3.0 vol %.

2.2. Fabrication of GWF/Epoxy Composites. The fabrication of GWF/epoxy composites involved preparation and infiltration of epoxy, two-step curing process, and etching of Ni template, as schematically illustrated in Figure 1. The epoxy resin consisted of four components: LY 1564, Aradure 1571, accelerator LY 1573, and hardener XB 3403 (supplied by Huntsman), in the weight ratio of 100:23:3:12. Acetone was used as solvent to adjust the viscosity of resin solution. After evaporation of solvent and degassing in a vacuum oven at 60 °C for 2 h, the epoxy resin was applied to impregnate the graphene/Ni woven fabrics. The composites were cured in a hot press at 80 °C for 30 min followed by 120 °C for 2 h to obtain ∼100 μm thick composites with a single layer of graphene/Ni woven fabric. The composite prepregs were immersed in dilute HCl (3 M) at 80 °C to etch the Ni template and cleaned by DI water, followed by drying in an oven at 60 °C overnight. GWF/epoxy composites with different graphene contents ranging from 0.19 to 0.62 wt % were prepared using GWFs with different numbers of graphene layers. "Porous epoxy" samples containing hollow channels were also prepared by applying epoxy resin directly onto the Ni template and etching Ni.

2.3. Characterization and Mechanical Tests. An optical microscope (Olympus BX51M), scanning electron microscopes (SEM, JEOL JSM-6390F, and JEOL JSM-6700F) with a 5 kV accelerating voltage, and a field emission transmission electron microscope (FETEM, JEOL 2010F) at an acceleration voltage of 200 kV were used to characterize the morphologies of freestanding GWFs and composites fracture surfaces. The defect contents of GWFs were evaluated by measuring the 2D- to G-band intensity ratios, I_{2D}/I_G, and the full width at half-maximum (fwhm) values of 2D peaks on a Micro-Raman spectrometer (Renishaw MicroRaman/Photoluminescence System) with Ar laser excitation of 514.5 nm wavelength. The tensile tests were carried out using 30 mm long x 5 mm wide rectangular composite films on a universal testing machine (MTS Alliance RT-5).[23,39]

The double edge notched tension (DENT) test was performed to measure the fracture resistance of solid epoxy, porous epoxy, and GWF/epoxy composites in mode I tension. The specimens were prepared according to the specifications, ASTM E399, whose dimensions are shown in Figure 2, where w = 13 mm, 2H = 26 mm, and the crack length to width ratio, a/w = 0.2.[40,41] The initial cracks were created using a sharp surgical blade. The DENT test was conducted on a universal testing machine (MTS Alliance RT/5) at a crosshead speed of 1 mm/min while monitoring the load−displace-

DOI: 10.1021/acsami.5b06476
ACS Appl. Mater. Interfaces 2015, 7, 21455−21464

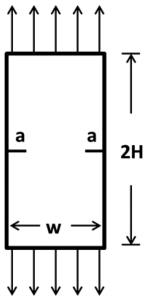

Figure 2. Geometry and dimension of a double edge notched tension (DENT) specimen.

ment curves. At least 5 specimens were tested for each set of conditions. The critical stress intensity factor, K_{Ic}, was calculated using eqs 1 and 2 when the external stress reached a critical value, σ_c, for crack propagation:

$$K_{Ic} = \sigma_c \sqrt{\pi a} F(a/w) \quad (1)$$

where $F(a/w)$ is a geometric correction factor and is given for a DENT specimen:[42]

$$F(a/w) = 1.12 + 0.41(a/w) - 4.78(a/w)^2 + 15.44(a/w)^3 \quad (2)$$

The fracture processes of specimens were in situ examined under an optical microscope with a video camera to monitor the crack propagation.

3. RESULTS AND DISCUSSION

3.1. Properties and Morphologies of GWFs. The mesh configuration and structural stability of GWFs depend on weave densities of the Ni templates. The SEM images of freestanding GWFs in three different configurations are presented in Figure 3. The GTs grown on thicker Ni wires (Figure 3a) were easily collapsed and the graphene layers were shrunk due to the large internal hollow space created after Ni etching. We chose the Ni woven fabrics with the finest mesh configuration having 200 meshes in a 25.4 × 25.4 mm^2 square and Ni wires of 56 μm in diameter (Figure 3c) for structural studies and composite fabrication.

During the heating and thermal annealing, the Ni template surface effectively functioned as catalyst for decomposition of carbon atoms from CH_4, which segregated on the Ni surface during rapid cooling to form graphene layers. The SEM images of GWF grown on the Ni template with 200 meshes with 0.5 vol % CH_4 flow (Figure 4) present high quality GTs that were complete without rupture or defects. While folds were formed along the tube direction as white lines in Figure 4b, the GWF had a well-preserved mesh structure where the GTs were interconnected at intercross points in the orthogonal directions. It is clearly seen (Figure 4c) that the graphene sheet had wrinkles representing the grain boundaries on the surface of Ni-WF template.

The Raman spectra (Figure 5a) are compared between the CVD-grown GFs[32] and the current GWFs, which likewise present prominent G- and 2D-band peaks at ~1580 and ~2700 cm^{-1}, respectively. They correspond to characteristic peaks for typical graphene. However, no D-band peaks were found at ~1350 cm^{-1}, a reflection of virtually no defects in the CVD-grown graphene. It is worth noting that the intensity of the unimodal 2D-peak in the GWF obtained at 0.5 vol % CH_4 was marginally stronger than the G-peak with an intensity ratio of $I_{2D}/I_G \approx 2$, indicating a few-layer graphene (see the corresponding TEM image from Figure 5c) similar to GFs obtained at 1.4 vol % CH_4 (Figure 5b).[32] With increasing CH_4 feed rate during the deposition step, the intensity of 2D-band became lower than that of G-band and the resultant number of graphene layers increased: e.g., when the CH_4 feed rate was increased to 3.0 vol %, the number of graphene layers increased up to ~12 layers (Figure 5d). Important factors that determine the number of graphene layers in the CVD process include the precursor gas concentration, the reaction temperature and time, and the cooling rate.

3.2. Physical and Electrical Properties of GWF/Epoxy Composites. The densities of GWF/epoxy composites and "porous epoxy" were determined from the known densities of solid epoxy (1.19 g/cm^3) and graphene (2.2 g/cm^3), graphene contents and the measured weights/volumes of the porous structures. The densities of both pore structures varied typically within a very narrow range 1.04−1.05 due to the presence of interconnected pores with porosities in the range of 12.5−12.3 vol % when the graphene content was changed between 0−0.62 wt %. The pore volume of the current GWF/epoxy composites is considered lower than 19.3 vol % of the GF/epoxy composites studied previously.[32]

The electrical conductivities of GWF/epoxy composites measured in the plane direction are plotted as a function of graphene content in Figure 6a. Compared with the pristine epoxy resin (~10^{-12} S/cm),[43] the electrical conductivity of the composite with 0.19 wt % graphene proliferated to 0.15 S/cm, corresponding to over 11 orders of magnitude improvement. The prompt transition from the insulating polymer to a conductive composite was realized by the addition of interconnected GWF structure. The orthogonally interconnected hollow GTs facilitated establishing a conductive network (shown in Figure 4a) with inherent percolation, which was responsible for the excellent electrical conductivities of the composites. When the graphene content was gradually

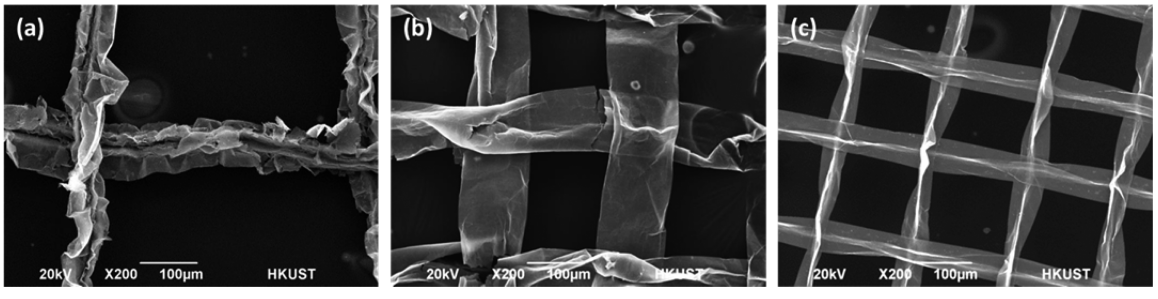

Figure 3. SEM images of freestanding GWFs grown on three Ni templates with different mesh densities and diameters: (a) 40 mesh, ⌀ = 130 μm; (b) 100 mesh, ⌀ = 80 μm; and (c) 200 mesh, ⌀ = 56 μm.

DOI: 10.1021/acsami.5b06476
ACS Appl. Mater. Interfaces 2015, 7, 21455−21464

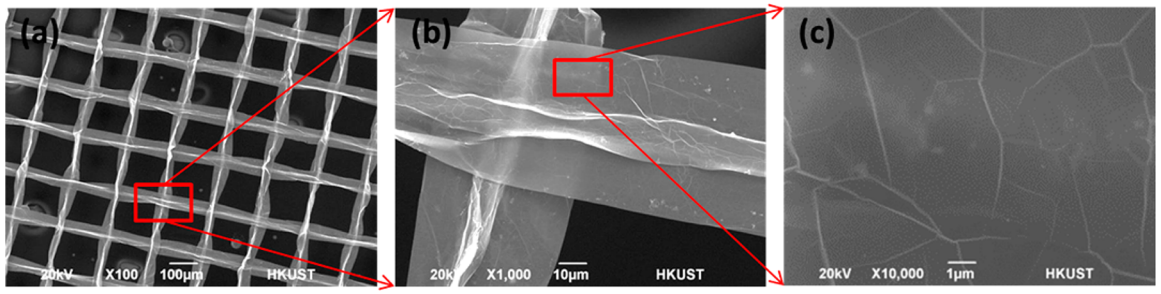

Figure 4. SEM images of freestanding GWF grown at a CH_4 concentration of 0.5 vol %.

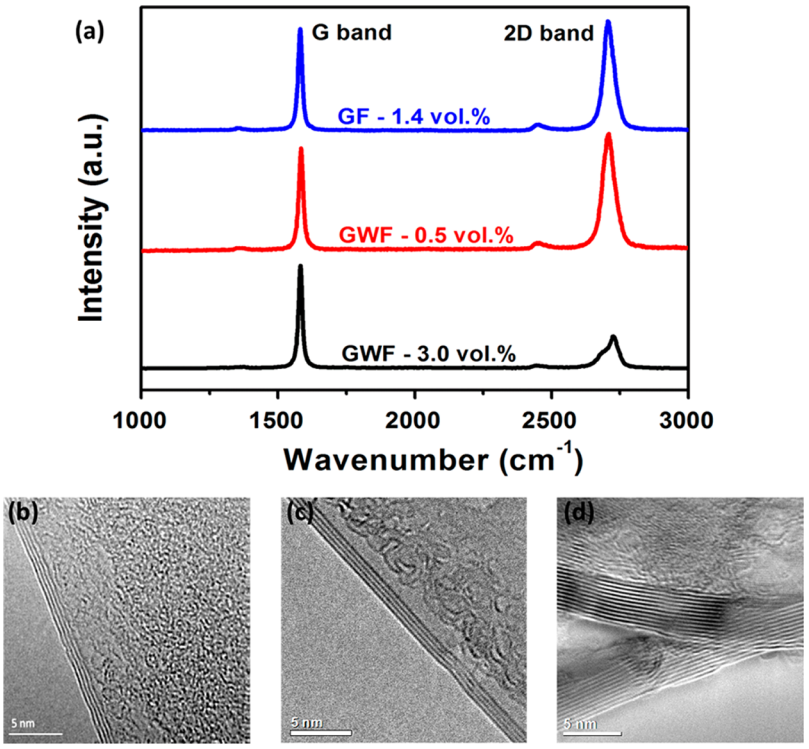

Figure 5. (a) Raman spectra of GF grown at 1.4 vol % CH_4,[32] GWFs grown at two different CH_4 concentrations of 0.5 and 3.0 vol %; (b–d) TEM images of GF grown at 1.4 vol % CH_4, and GWFs grown at two different CH_4 concentrations of 0.5 and 3.0 vol %, respectively.

increased, however, the electrical conductivities of the composites did not exhibit a commensurate increase, i.e., from 0.15 to ~0.18 S/cm, with increasing the graphene content from 0.19 to 0.62 wt %. Unlike the composites made from individual graphene sheets dispersed in a polymer matrix, a higher graphene content in GWF/epoxy composites means only a moderately increased thickness of the already percolated GTs without creating extra conducting channels. Regardless of graphene content, the marked enhancement in electrical conductivity of GWF/epoxy composites directly benefited from the defect-free GWF prepared in this study. Superimposed in Figure 6a are the electrical conductivities of freestanding GWFs, which are over a magnitude higher than those of their composites. It is found previously that the GFs with an average five layers graphene had the highest electrical conductivities among freestanding GFs and GF/PDMS composites with different graphene contents.[31] Similarly, the electrical conductivities of GWFs did not display a monotonic increase with CH_4 concentration, and instead, they varied in a narrow range between 2.3 and 2.9 S/cm.

A comparison of electrical conductivities between the current work and similar epoxy (EP)-based composites containing different types of carbon fillers, including 3D graphene structures and 2D rGO layers, 1D CNTs and carbon nanofibers (CNFs), is presented in Figure 6b. The current study on GWF/epoxy composites revealed phenomenal electrical conductivities at relatively low filler contents, which are at least 3 orders of magnitude higher than those of the composites with GNP,[44] rGO,[24] CNTs,[45,46] and CNFs,[47] benefiting from the interconnected conductive channels naturally constituted by the high-quality hollow GTs. The GWF/epoxy composites boasted over 10 times higher electrical conductivities than the 3D GA/epoxy system[26] for a given graphene content, placing the former system the second most conductive after the 3D GF/epoxy composites.[32] It should be noted that both the CVD-grown GWFs and GFs are interconnected by GTs to form inherent percolation and contain high quality graphene, requiring no extra reduction process to remove the insulating oxygenated functional groups so as to restore the inherently high conductivities of graphene.

DOI: 10.1021/acsami.5b06476
ACS Appl. Mater. Interfaces 2015, 7, 21455–21464

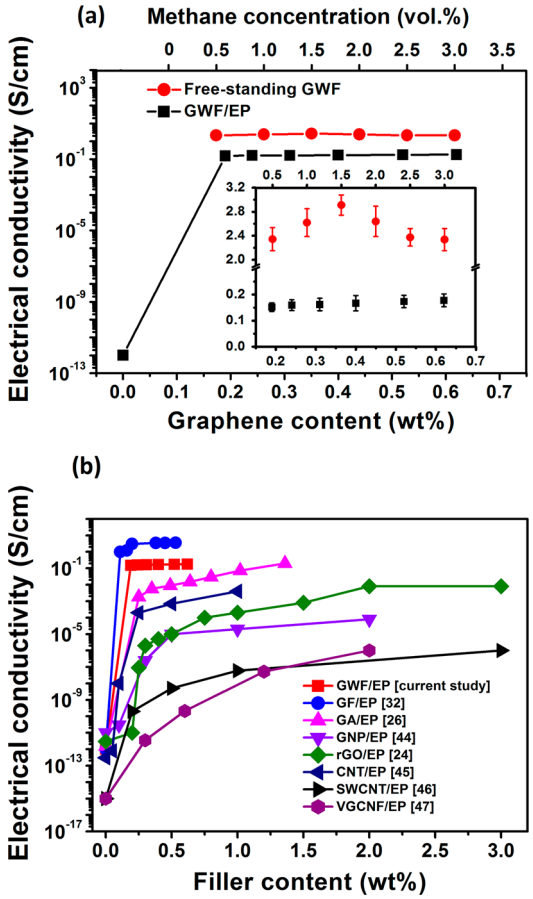

Figure 6. (a) In-plane electrical conductivities of GWF/epoxy composites and freestanding GWFs; (b) comparison of electrical conductivities of epoxy-based composites with different carbon fillers.

3.4. Fracture Toughness and Tensile Properties of GWF/Epoxy Composites. The porous epoxy and GWF/epoxy composites showed significant anisotropy in fracture and mechanical properties because the hollow GTs are interconnected in two orthogonal directions. Therefore, the effect of GT orientation relative to the loading direction should be taken into consideration when evaluating their fracture behaviors and mechanical properties. The specimens with three different orientations were tested in this work: namely, 0° only, 45° only, and 0°/45°. Figure 7a illustrates the fracture toughness, K_{Ic}, of solid epoxy, porous epoxy and GWF/epoxy composites plotted as a function of graphene loading. K_{Ic} of solid epoxy was 1.07 MPa·m$^{1/2}$, consistent with the reported values of similar epoxy systems.[48] When the hollow tubes were present orthogonal to the external force, i.e. 0°, K_{Ic} of porous epoxy without graphene increased to 1.21 MPa·m$^{1/2}$, about 13% higher than that of the solid epoxy. The fracture toughness of the GWF/epoxy composites gradually increased with increasing graphene content to 1.67 MPa·m$^{1/2}$ with 0.62 wt % graphene at 0°, equivalent to about 38% and 57% improvements compared to the corresponding values of the porous epoxy and solid epoxy, respectively. It is worth noting that when the tubes were positioned 45° to the applied load the porous epoxy and the GWF/epoxy composites displayed consistently higher fracture toughness than those with the 0° orientation by about 0.1 MPa·m$^{1/2}$ for all graphene contents studied. Thus, the K_{Ic} values of the porous epoxy and 0.62 wt % GWF/epoxy composite were 1.34 and 1.78 MPa·m$^{1/2}$, approximately 25% and 67% surges

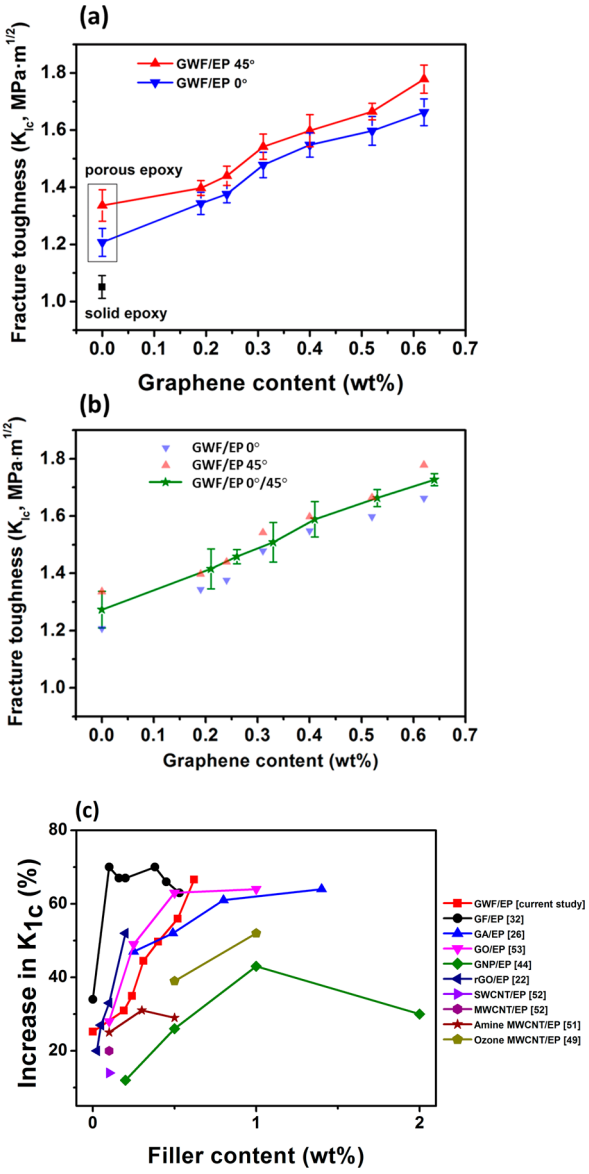

Figure 7. Mode I fracture toughness K_{Ic} of (a) GWF/epoxy composites loaded in two different directions; (b) GWF/epoxy composites containing 0° and 45° layers as a function of graphene content; and (c) comparison of fracture toughness of epoxy-based composites with different types of nanocarbon fillers.

compared with the solid epoxy, respectively. Figure 7b presents the fracture toughness of GWF/epoxy composites containing 0°/45° mixed tube orientations. Interestingly, their fracture toughness values varied approximately between those of the composites made from 0° and 45° GWFs.

To identify the standing of the GWF composites among peers reinforced with other forms of carbon fillers, the fracture toughness values are compared between the similar epoxy-based composites containing GFs, GAs, GNPs, and single-walled and multiwalled CNTs with different surface functionalization taken from the literature, as shown in Figure 7c. To eliminate the influence of slightly different fracture toughness values of different epoxy systems as the matrix, only the % increments against those obtained for their respective neat epoxy systems are compared. Among the various CNT/epoxy composites, the highest increase in K_{Ic} was 52% at 1.0 wt % reported for the CNTs with ozone treatment,[49] although there

DOI: 10.1021/acsami.5b06476
ACS Appl. Mater. Interfaces 2015, 7, 21455−21464

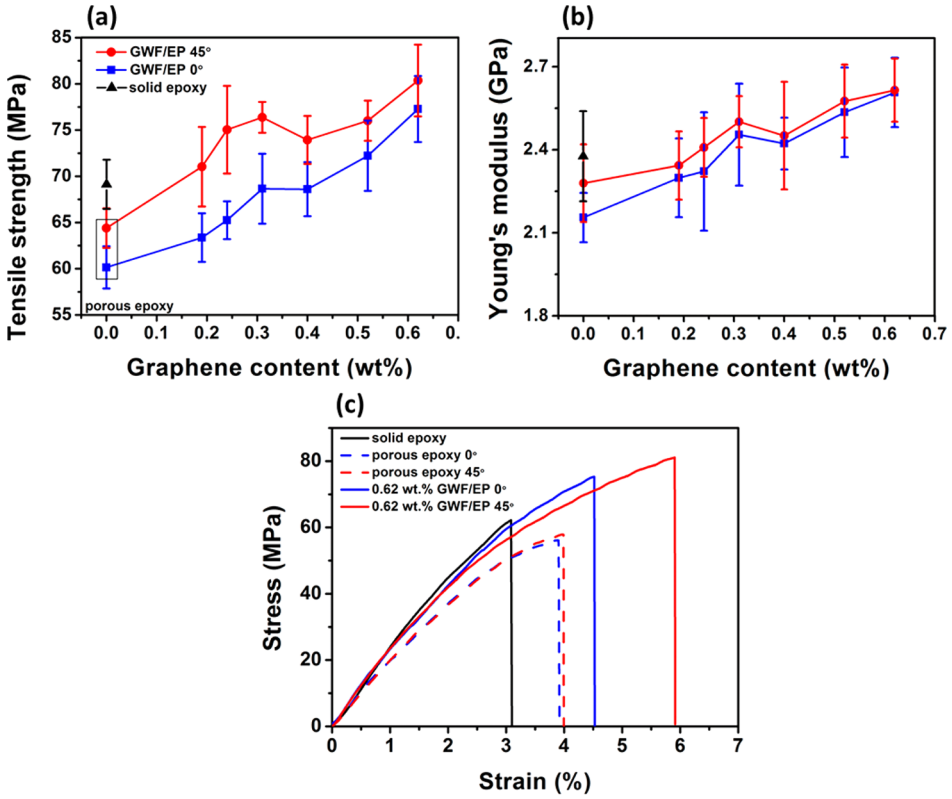

Figure 8. (a) Tensile strength and (b) Young's modulus of solid epoxy, porous epoxy, and GWF/epoxy composites as a function of graphene content; (c) typical strain–stress curves of solid epoxy, porous epoxy, and GWF/epoxy composites at 0.62 wt % graphene at two different loading directions.

was a report on 58% improvement in impact fracture toughness of CNT/epoxy composites with only 0.25 wt % of surfactant-treated MWCNTs.[50] After amino-functionalization, the MWCNT/epoxy composites delivered 31% increase in K_{Ic} at 0.3 wt % filler loading.[51] Without functionalization, the MWCNTs and SWCNTs showed marginal enhancements, just about 20% and 14%, respectively,[52] a reflection of the importance of CNT functionalization. GNPs offered large improvements in fracture toughness over a range of filler content from 0.3 to 2.0 wt %, with typically 43% enhancement at 1.0 wt % GNP.[44] Well-dispersed GO and rGO sheets performed better than GNPs and CNTs with 49 and 52% increases with 0.25 wt %[53] and 0.2 wt %,[22] respectively, due to the presence of oxygenated functional groups on their basal planes and edges allowing $\pi-\pi$ interactions or covalent bonds with the epoxy matrix. However, the fracture resistance of the composites containing 1D CNTs or 2D graphene nanosheets was always dependent on their dispersion states. Although the relative performance of the GWF/epoxy composites was not impressive compared to the GO/and rGO/epoxy composites at low filler contents, say below 0.5 wt %, they delivered the highest increment in K_{Ic} at a high filler content above 0.62 wt % among all composites studied and even higher than GF counterparts.

Figure 8 presents the tensile strength and Young's modulus of epoxy and GWF/epoxy composites with 0° and 45° orientations. In contrast to the aforementioned fracture toughness, the porous epoxy was sharply weaker and less stiff than the solid epoxy, due mainly to the presence of hollow tubes of a large volume fraction. The hollow tubes without graphene walls disturbed the continuity of stress transfer through the bulk matrix. With the incorporation of graphene, however, both the tensile strength and modulus of the composites were quickly recovered, and they consistently increased with increasing graphene content. Typical strain–stress curves of solid epoxy, porous epoxy and GWF/epoxy composite with 0.62 wt % graphene at 0° and 45° are shown in Figure 8c. Compared with the almost linear elasticity of solid epoxy, the porous epoxy and GWF/epoxy composites presented large deformation and nonlinear curves at high strains. Thus, at 0.62 wt % graphene, their tensile strengths with 0° and 45° orientations were ~12% and ~16% higher than those of the solid epoxy, respectively. The seamlessly interconnected graphene layers in the GTs contributed significantly to the strength and modulus of the composites due to its extremely high strength (~130 GPa) and modulus (~1.0 TPa).[54] The continuous and defect-free GTs can be considered hollow and strong/stiff/tough fibers. However, the predictions based on a simple rule of mixtures equation overestimate these mechanical properties compared to the experimental data because the stress concentrations arising from the hollow inside of GTs cannot be properly taken into account in the predictions. Another reason for the mild enhancements in mechanical properties may arise from the weak interfacial bonds between the GTs and epoxy resin because of no prior functionalization of CVD-grown graphene.[32] The higher strengths and moduli of the composites with 45° inclined GTs than those with 0° GTs is because a relatively larger number of GTs could contribute to these mechanical properties in the former geometry in tension. At 0°, the GTs paralleled to the applied force only played a dominant reinforcement role, while at 45°, the GTs in the two directions

DOI: 10.1021/acsami.5b06476
ACS Appl. Mater. Interfaces 2015, 7, 21455–21464

both contributed to the enhancement of strength and modulus. It is interesting to note that the differences in strength and modulus between the composites with different graphene tube orientations were generally larger at low graphene contents. Relative to the notable changes in strength, the Young's modulus of the composites showed only moderate improvements and the difference between the two orientations was relatively small.

3.5. Toughening Mechanisms of GWF/Epoxy Composites. It has been reported that crack pinning, debonding, pull-out, and crack tip bridging are the main fracture mechanisms in CNT-reinforced epoxy composites,[55] whereas crack deflections and debonding between the fillers and matrix are the most important failure mechanisms for the composites containing 2D graphene nanosheets.[56,57] However, no obvious evidence of crack pinning or crack deflection mechanism was found in the GWF/epoxy composites. For the porous epoxy and GWF/epoxy composites, the interconnected hollow tubes and graphene layers played significant roles in fracture behavior.

Distinct and unique features were identified from the fracture surfaces of the specimens, as exhibited in Figure 9. Compared with the smooth fracture surface of the solid epoxy (Figure 9a), the porous epoxy showed a microscopically rougher surface, especially around the hollow tubes where the running crack tips were interrupted and became blunted before tearing open the tubes along the longitudinal direction (Figure 9b). The deformation and collapse of the hollow tubes, and the increasing surface roughness mean higher fracture resistance of the porous epoxy than the solid epoxy. With the reinforcement of GTs, the fracture surface became even rougher (Figures 9c,d) and there were signs of significant deformation of the matrix surrounding the GTs (Figures 9e,f). Tearing off the strong/stiff graphene layers along the tube direction required more energy to dissipate during the fracture of GTs. The interfacial debonding and sliding of graphene layers at high graphene contents, especially in the absence of any prior functionalization (Figure 9d), may partly contribute to higher fracture toughness.

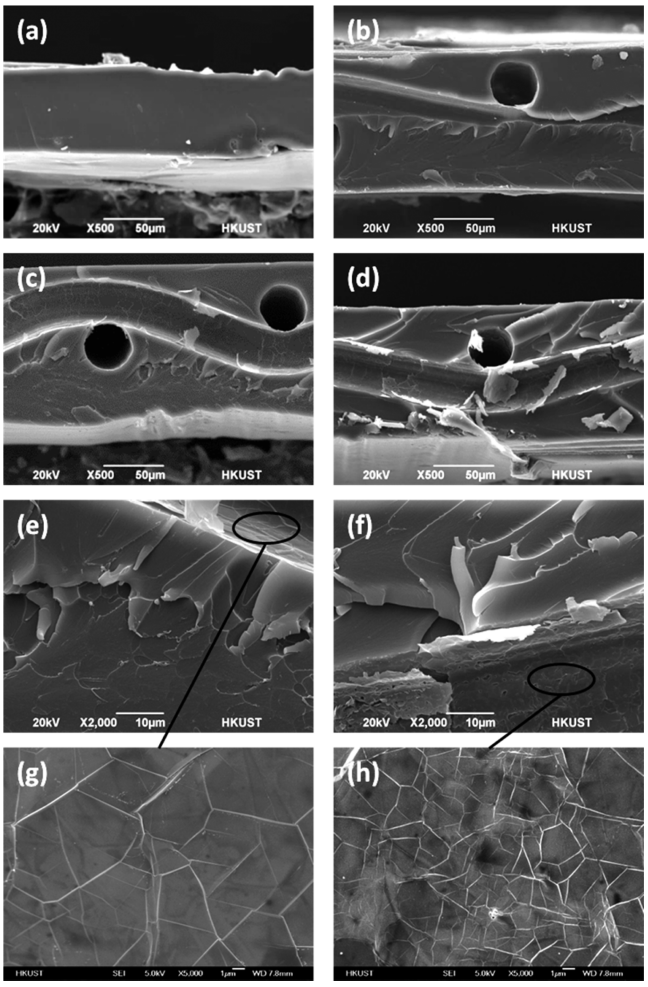

Figure 9. SEM images of fracture surfaces of (a) solid epoxy, (b) porous epoxy, GWF/epoxy composites with 0.19 and 0.62 wt % graphene contents (c, d) at a low magnification and (e, f) at a high magnification. The crack propagation direction is from left to right. (g, h) graphene surface in (e, f).

Based on the above observations, the interactions between the crack tips and hollow tubes with and without reinforcing graphene layers during fracture are identified as follows. (i) The hollow tubes, both with and without graphene, which run parallel to the external load (or perpendicular to the crack tip direction) functioned as a discrete phase to resist crack propagation. The porous configuration and the graphene layers surrounding the tubes constrained crack extension, blunting the crack tip by terminating it or changing its direction and moving slowly.[58] (ii) The hollow tubes decreased the stress-concentration at the blunted crack tip. The epoxy matrix surrounding the hollow tubes underwent large deformation, requiring a higher external force and energy for crack extension.[59] (iii) Once the deflected crack reached the tube running perpendicular to the external force (or along the initial crack direction), the crack tended to propagate along its longitudinal direction by tearing it because of the largely reduced ligament area requiring a much reduced force for crack extension. Besides the porous structure, the pronounced enhancements in fracture toughness arose from crack-tip blunting offered by the presence of graphene layers in the composite. (iv) The GTs functioned as fortified walls to maintain and strengthen the hollow tubes. Interfacial debonding and sliding between graphene layers and epoxy matrix took place during tearing of these hollow tubes, allowing additional energies to dissipate during the process. Apart from crack tip blunting and higher tearing forces, debonding and frictional sliding ameliorated the crack growth resistance in the GWF/epoxy composites. It appears that these toughening mechanisms became more pronounced as the graphene content increased, which is responsible for consistently enhanced toughness with graphene content.

In light of the above discussion, schematics are presented of crack propagation behaviors in the solid epoxy and the GWF/epoxy composites with initial cracks. Here, the crack propagation behavior of porous epoxy is considered much the same as the GWF/epoxy composites. Their load–displacement curves are shown in Figure 10a and the matching crack propagation behaviors are schematically drawn in Figure 10c,d with reference to Movies 1 and 2 in the Supporting Information. The crack in the solid epoxy extends right through the specimen braking into two pieces catastrophically without crack deflection (Figure 10b), a reflection of its brittle nature and the almost linear load-deflection curve in Figure 10a. The initial crack in the GWF/epoxy composite propagates quickly until it encounters the first GT which stops and blunts the running crack (stage II in Figure 10c,d). Then, the blunted

DOI: 10.1021/acsami.5b06476
ACS Appl. Mater. Interfaces 2015, 7, 21455–21464

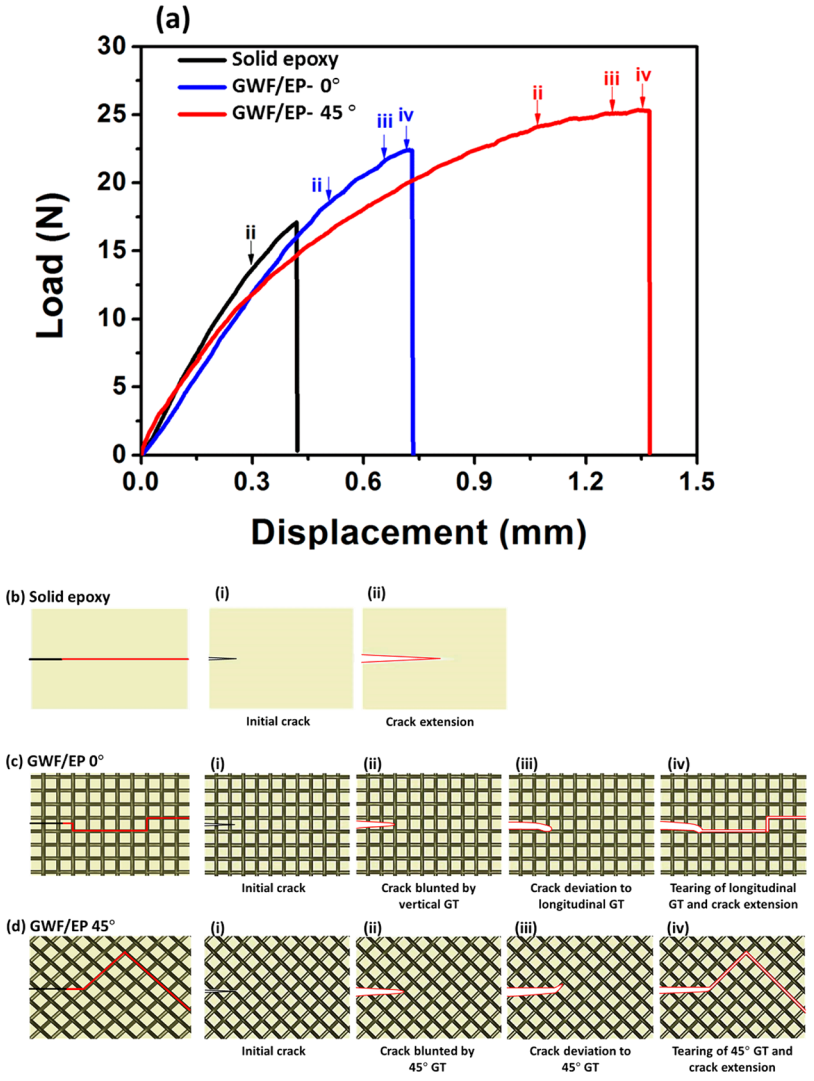

Figure 10. (a) Typical load−displacement curves of solid epoxy and GWF/epoxy composites obtained from the fracture tests. Schematics of fracture process and the details around crack tips in (b) solid epoxy, (c-d) GWF/epoxy composites with two different graphene tube orientations. The black lines are the initial cracks, and the red lines show the crack propagation paths.

crack tip is deviated toward the GT perpendicular or 45° to the external load (stage III in Figure 10c,d). Once there is a sufficient driving force, the crack propagates rapidly along the GT by tearing it off (stage IV in Figure 10c,d). It should be noted that the crack propagation behaviors are very sensitive to the direction of GTs relative to the external force. In the composites with the GTs running 0° and 90° directions, the crack propagation is limited by the tubes transverse to the running cracks. Then, the crack jumps to an adjacent tube that runs perpendicular to the external load (Figure 10c). In the composites with the tubes arranged 45° to the external load, the crack propagation is restricted immediately by the first tube encountered and the crack paths became a "zigzag" shape (Figure 10d). In this case, the driving force for tearing the hollow tubes should be higher than that required for the above composites with 0° GTs, according to the von Mises criterion and thus higher fracture toughness than the 0° samples.

4. CONCLUSION

Interconnected GWFs consisting of orthogonal GTs were synthesized by template-based CVD process, and the GWF/epoxy composites were prepared by casting epoxy resin with GWFs. The combination of excellent electrical conductivity and mechanical strength/modulus of GWFs make them ideal conductive and toughening filler, improving the electrical, fracture, and mechanical properties of epoxy-based composites. The properties of GWFs and their composites were characterized and the following results can be highlighted from the experimental study:

(i) The GWFs synthesized on Ni woven fabric templates consisted of hollow GTs arranged at right angles in a mesh configuration. Grown under 0.5−3.0 vol % methane concentrations, the average numbers of graphene layers in GWFs varied between 4 and 12. GWF/epoxy composites were fabricated containing an almost uniform porosity of ∼ 12.4 vol % and different graphene contents of 0−0.62 wt %.

(ii) The as-prepared GWFs had inherently percolated conducting networks. A high electrical conductivity of 2.9 S/cm was achieved for freestanding GWF with ∼7 layers of graphene prepared by 1.5 vol % CH_4, and the corresponding conductivity of the GWF/epoxy composite was 0.16 S/cm. The interconnected network of high quality GTs means that the GWF/epoxy composites can

DOI: 10.1021/acsami.5b06476
ACS Appl. Mater. Interfaces 2015, 7, 21455−21464

totally eliminate the difficulties for uniform dispersion of chemically exfoliated GO sheets in polymer and the additional reduction processes to restore their conductivities.

(iii) The orientations of hollow tubes in the porous epoxy and GWF/epoxy composites relative to the loading direction were taken into account when their fracture behavior and mechanical properties were characterized. The porous epoxy possessed fracture toughness of 1.21 and 1.34 MPa·$m^{1/2}$ at 0° and 45° orientations, about 13% and 25% enhancements against the solid epoxy, respectively. The GWF/epoxy composites delivered the highest K_{Ic} values of 1.67 and 1.78 MPa·$m^{1/2}$ at 0.62 wt % graphene in the two directions, respectively, equivalent to remarkable 57% and 67% surges compared to the solid epoxy. At 0.62 wt % graphene loading, the tensile strengths of the composites with these two orientations were about 12% and 16% higher than the solid epoxy.

(iv) The considerable improvement in fracture toughness of the composites is mainly attributed to the crack tip blunting effect caused by the porous GTs, especially those at 45° to the running crack, as well as tearing of GTs along the longitudinal direction, debonding, and frictional sliding between the graphene layers and epoxy matrix.

■ ASSOCIATED CONTENT

Supporting Information

The Supporting Information is available free of charge on the ACS Publications website at DOI: 10.1021/acsami.5b06476.

Movie 1: Fracture process and the details around crack tips of GWF/epoxy composite at 0°(ZIP)

Movie 2: Fracture process and the details around crack tips of GWF/epoxy composite at 45°(ZIP)

■ AUTHOR INFORMATION

Corresponding Author

*Fax: +852 2358 1543. E-mail: mejkkim@ust.hk.

Notes

The authors declare no competing financial interest.

■ ACKNOWLEDGMENTS

This project was financially supported by the Research Grants Council of Hong Kong SAR (GRF Projects 16212814 and 16203415). The authors also appreciate the technical assistance from the Advanced Engineering Materials Facilities (AEMF) and the Materials Characterization and Preparation Facilities (MCPF) of HKUST.

■ REFERENCES

(1) Novoselov, K. S.; Fal'ko, V. I.; Colombo, L.; Gellert, P. R.; Schwab, M. G.; Kim, K. A Roadmap for Graphene. *Nature* **2012**, *490* (7419), 192−200.

(2) Geim, A. K.; Novoselov, K. S. The Rise of Graphene. *Nat. Mater.* **2007**, *6* (3), 183−191.

(3) Singh, V.; Joung, D.; Zhai, L.; Das, S.; Khondaker, S. I.; Seal, S. Graphene Based materials: Past, Present and Future. *Prog. Mater. Sci.* **2011**, *56* (8), 1178−1271.

(4) Balandin, A. A. Thermal Properties of Graphene and Nanostructured Carbon Materials. *Nat. Mater.* **2011**, *10* (8), 569−581.

(5) Nika, D. L.; Balandin, A. A. Two-Dimensional Phonon Transport in Graphene. *J. Phys.: Condens. Matter* **2012**, *24* (23), 233203.

(6) Stankovich, S.; Dikin, D. A.; Dommett, G. H. B.; Kohlhaas, K. M.; Zimney, E. J.; Stach, E. A.; Piner, R. D.; Nguyen, S. T.; Ruoff, R. S. Graphene-Based Composite Materials. *Nature* **2006**, *442* (7100), 282−286.

(7) Potts, J. R.; Dreyer, D. R.; Bielawski, C. W.; Ruoff, R. S. Graphene-Based Polymer Nanocomposites. *Polymer* **2011**, *52* (1), 5−25.

(8) Hu, K.; Kulkarni, D. D.; Choi, I.; Tsukruk, V. V. Graphene-Polymer nanocomposites for structural and functional applications. *Prog. Polym. Sci.* **2014**, *39* (11), 1−39.

(9) Yousefi, N.; Sun, X.; Lin, X.; Shen, X.; Jia, J.; Zhang, B.; Tang, B.; Chan, M.; Kim, J.-K. Highly Aligned Graphene/Polymer Nanocomposites with Excellent Dielectric Properties for High-Performance Electromagnetic Interference Shielding. *Adv. Mater.* **2014**, *26* (31), 5480−5487.

(10) Zhang, B.; Zheng, Q. B.; Huang, Z. D.; Oh, S. W.; Kim, J. K. SnO_2-Graphene-Carbon Nanotube Mixture for Anode Material with Improved Rate Capacities. *Carbon* **2011**, *49* (13), 4524−4534.

(11) Huang, Z.-D.; Zhang, B.; Oh, S.-W.; Zheng, Q.-B.; Lin, X.-Y.; Yousefi, N.; Kim, J.-K. Self-Assembled Graphene Oxide/Carbon Nanotube Films as Electrodes for Supercapacitors. *J. Mater. Chem.* **2012**, *22* (8), 3591−3599.

(12) Shahil, K. M. F.; Balandin, A. A. Graphene-Multilayer Graphene Nanocomposites as Highly Efficient Thermal Interface Materials. *Nano Lett.* **2012**, *12* (2), 861−867.

(13) Renteria, J. D.; Nika, D. L.; Balandin, A. A. Graphene Thermal Properties: Applications in Thermal Management and Energy Storage. *Appl. Sci.* **2014**, *4* (4), 525−547.

(14) Malekpour, H.; Chang, K.-H.; Chen, J.-C.; Lu, C.-Y.; Nika, D. L.; Novoselov, K. S.; Balandin, A. A. Thermal Conductivity of Graphene Laminate. *Nano Lett.* **2014**, *14* (9), 5155−5161.

(15) Renteria, J. D.; Ramirez, S.; Malekpour, H.; Alonso, B.; Centeno, A.; Zurutuza, A.; Cocemasov, A. I.; Nika, D. L.; Balandin, A. A. Strongly Anisotropic Thermal Conductivity of Free-Standing Reduced Graphene Oxide Films Annealed at High Temperature. *Adv. Funct. Mater.* **2015**, *25* (29), 4664−4672.

(16) Al-Mashat, L.; Shin, K.; Kalantar-zadeh, K.; Plessis, J. D.; Han, S. H.; Kojima, R. W.; Kaner, R. B.; Li, D.; Gou, X.; Ippolito, S. J.; Wlodarski, W. Graphene/Polyaniline Nanocomposite for Hydrogen Sensing. *J. Phys. Chem. C* **2010**, *114* (39), 16168−16173.

(17) Konwer, S.; Guha, A. K.; Dolui, S. K. Graphene Oxide-Filled Conducting Polyaniline Composites as Methanol-Sensing Materials. *J. Mater. Sci.* **2013**, *48* (4), 1729−1739.

(18) Bae, S.-H.; Lee, Y.; Sharma, B. K.; Lee, H.-J.; Kim, J.-H.; Ahn, J.-H. Graphene-based Transparent Strain Sensor. *Carbon* **2013**, *51*, 236−242.

(19) Lin, X.; Shen, X.; Zheng, Q.; Yousefi, N.; Ye, L.; Mai, Y.-W.; Kim, J.-K. Fabrication of Highly-Aligned, Conductive, and Strong Graphene Papers Using Ultralarge Graphene Oxide Sheets. *ACS Nano* **2012**, *6* (12), 10708−10719.

(20) Li, J.; Sham, M. L.; Kim, J.-K.; Marom, G. Morphology and Properties of UV/Ozone Treated Graphite Nanoplatelet/Epoxy Nanocomposites. *Compos. Sci. Technol.* **2007**, *67* (2), 296−305.

(21) Hu, H.; Wang, X.; Wang, J.; Wan, L.; Liu, F.; Zheng, H.; Chen, R.; Xu, C. Preparation and Properties of Graphene Nanosheets-Polystyrene Nanocomposites via in situ Emulsion Polymerization. *Chem. Phys. Lett.* **2010**, *484* (4), 247−253.

(22) Tang, L.-C.; Wan, Y.-J.; Yan, D.; Pei, Y.-B.; Zhao, L.; Li, Y.-B.; Wu, L.-B; Jiang, J.-X.; Lai, G.-Q. The Effect of Graphene Dispersion on the Mechanical Properties of Graphene/Epoxy Composites. *Carbon* **2013**, *60*, 16−27.

(23) Yousefi, N.; Gudarzi, M. M.; Zheng, Q.; Lin, X.; Shen, X.; Jia, J.; Sharif, F.; Kim, J.-K. Highly Aligned, Ultralarge-Size Reduced Graphene Oxide/Polyurethane Nanocomposites: Mechanical Properties and Moisture Permeability. *Composites, Part A* **2013**, *49*, 42−50.

(24) Yousefi, N.; Lin, X.; Zheng, Q.; Shen, X.; Pothnis, J. R.; Jia, J.; Zussman, E.; Kim, J.-K. Simultaneous in situ Reduction, Self-Alignment and Covalent Bonding in Graphene Oxide/Epoxy Composites. *Carbon* **2013**, *59*, 406−417.

DOI: 10.1021/acsami.5b06476
ACS Appl. Mater. Interfaces 2015, 7, 21455−21464

(25) Li, W.; Tang, X.-Z.; Zhang, H.-B; Jiang, Z.-G.; Yu, Z.-Z.; Du, X.-S.; Mai, Y.-W. Simultaneous Surface Functionalization and Reduction of Graphene Oxide with Octadecylamine for Electrically Conductive Polystyrene Composites. *Carbon* **2011**, *49* (14), 4724−4730.
(26) Wang, Z.; Shen, X.; Garakani, M. A.; Lin, X.; Wu, Y.; Liu, X.; Sun, X.; Kim, J.-K. Graphene Aerogel/Epoxy Composites with Exceptional Anisotropic Structure and Properties. *ACS Appl. Mater. Interfaces* **2015**, *7* (9), 5538−5549.
(27) Worsley, M. A.; Pauzauskie, P. J.; Olson, T. Y.; Biener, J.; Satcher, J. H.; Baumann, T. F. Synthesis of Graphene Aerogel with High Electrical Conductivity. *J. Am. Chem. Soc.* **2010**, *132* (40), 14067−14069.
(28) Hu, H.; Zhao, Z.; Wan, W.; Gogotsi, Y.; Qiu, J. Ultralight and Highly Compressible Graphene Aerogels. *Adv. Mater.* **2013**, *25* (15), 2219−2223.
(29) Chen, Z.; Xu, C.; Ma, C.; Ren, W.; Cheng, H.-M. Lightweight and Flexible Graphene Foam Composites for High-Performance Electromagnetic Interference Shielding. *Adv. Mater.* **2013**, *25* (9), 1296−1300.
(30) Dong, X.; Wang, X.; Wang, L.; Song, H.; Zhang, H.; Huang, W.; Chen, P. 3D Graphene Foam as a Monolithic and Macroporous Carbon Electrode for Electrochemical Sensing. *ACS Appl. Mater. Interfaces* **2012**, *4* (6), 3129−3133.
(31) Chen, Z.; Ren, W.; Gao, L.; Liu, B.; Pei, S.; Cheng, H.-M. Three-Dimensional Flexible and Conductive Interconnected Graphene Networks Grown by Chemical Vapor Deposition. *Nat. Mater.* **2011**, *10* (6), 424−428.
(32) Jia, J.; Sun, X.; Lin, X.; Shen, X.; Mai, Y.-W; Kim, J.-K. Exceptional Electrical Conductivity and Fracture Resistance of 3D Interconnected Graphene Foam/Epoxy Composites. *ACS Nano* **2014**, *8* (6), 5774−5783.
(33) Li, X.; Sun, P.; Fan, L.; Zhu, M.; Wang, K.; Zhong, M.; Wei, J.; Wu, D.; Cheng, Y.; Zhu, H. Multifunctional Graphene Woven Fabrics. *Sci. Rep.* **2012**, *2*, 395.
(34) Wang, Y.; Wang, L.; Yang, T.; Li, X.; Zang, X.; Zhu, M.; Wang, K.; Wu, D.; Zhu, H. Wearable and Highly Sensitive Graphene Strain Sensors for Human Motion Monitoring. *Adv. Funct. Mater.* **2014**, *24* (29), 4666−4670.
(35) Seah, C.-M.; Chai, S.-P.; Mohamed, A. R. Mechanisms of Graphene Growth by Chemical Vapor Deposition on Transition Metals. *Carbon* **2014**, *70*, 1−21.
(36) Li, X.; Zhang, R.; Yu, W.; Wang, K.; Wei, J.; Wu, D.; Cao, A.; Li, Z.; Cheng, Y.; Zheng, Q.; Ruoff, R. S.; Zhu, H. Stretchable and Highly Sensitive Graphene-on-Polymer Strain Sensors. *Sci. Rep.* **2012**, *2*, 870.
(37) Li, X.; Zang, X.; Li, Z.; Li, X.; Li, P.; Sun, P.; Lee, X.; Zhang, R.; Huang, Z.; Wang, K.; Wu, D.; Kang, F.; Zhu, H. Large-Area Flexible Core-Shell Graphene/Porous Carbon Woven Fabric Films for Fiber Supercapacitor Electrodes. *Adv. Funct. Mater.* **2013**, *23* (38), 4862−4869.
(38) Zang, X.; Chen, Q.; Li, P.; He, Y.; Li, X.; Zhu, M.; Li, X.; Wang, K.; Zhong, M.; Wu, D.; Zhu, H. Highly Flexible and Adaptable, All-Solid-State Supercapacitors Based on Graphene Woven-Fabric Film Electrodes. *Small* **2014**, *10* (13), 2583−2588.
(39) Cheng, Q.; Wu, M.; Li, M.; Jiang, L.; Tang, Z. Ultratough Artificial Nacre Based on Conjugated Cross-linked Graphene Oxide. *Angew. Chem., Int. Ed.* **2013**, *52* (13), 3750−3755.
(40) Uddin, M. N.; Huang, Z.-D.; Mai, Y.-W.; Kim, J.-K. Tensile and Tearing Fracture Properties of Graphene Oxide Papers Intercalated with Carbon Nanotubes. *Carbon* **2014**, *77*, 481−491.
(41) Seth, R. S.; Page, D. H. Fracture Resistance of Paper. *J. Mater. Sci.* **1974**, *9* (11), 1745−1753.
(42) Nestor, P. *Fracture Mechanics*; Kluwer Academic Publishers: New York, 2004; Chapter 3, p 48.
(43) Khan, S. U.; Pothnis, J. R.; Kim, J.-K. Effects of Carbon Nanotube Alignment on Electrical and Mechanical Properties of Epoxy Nanocomposites. *Composites, Part A* **2013**, *49*, 26−34.
(44) Chandrasekaran, S.; Seidel, C.; Schulte, K. Preparation and Characterization of Graphite Nano-Platelet (GNP)/epoxy Nano-Composite: Mechanical, Electrical and Thermal Properties. *Eur. Polym. J.* **2013**, *49* (12), 3878−3888.
(45) Li, J.; Ma, P. C.; Chow, W. S.; To, C. K.; Tang, B. Z.; Kim, J.-K. Correlations between Percolation Threshold, Dispersion State, and Aspect Ratio of Carbon Nanotubes. *Adv. Funct. Mater.* **2007**, *17* (16), 3207−3215.
(46) Wang, Q.; Dai, J.; Li, W.; Wei, Z.; Jiang, J. The Effects of CNT Alignment on Electrical Conductivity and Mechanical Properties of SWNT/epoxy Nanocomposites. *Compos. Sci. Technol.* **2008**, *68* (7), 1644−1648.
(47) Ardanuy, M.; Rodríguez-Perez, M. A.; Algaba, I. Electrical Conductivity and Mechanical Properties of Vapor-Grown Carbon Nanofibers/trifunctional Epoxy Composites Prepared by Direct Mixing. *Composites, Part B* **2011**, *42* (4), 675−681.
(48) Ma, P. C.; Kim, J.-K.; Tang, B. Z. Effects of Silane Functionalization on the Properties of Carbon Nanotube/epoxy Nanocomposites. *Compos. Sci. Technol.* **2007**, *67* (14), 2965−2972.
(49) Tang, L.-C.; Zhang, H.; Han, J.-H.; Wu, X.-P.; Zhang, Z. Fracture Mechanisms of Epoxy Filled with Ozone Functionalized Multi-Wall Carbon Nanotubes. *Compos. Sci. Technol.* **2011**, *72* (1), 7−13.
(50) Geng, Y.; Liu, M. Y.; Li, J.; Shi, X. M.; Kim, J. K. Effects of Surfactant Treatment on Mechanical and Electrical Properties of CNT/epoxy Nanocomposites. *Composites, Part A* **2008**, *39* (12), 1876−1883.
(51) Gojny, F. H.; Wichmann, M. H. G.; Fiedler, B.; Schulte, K. Influence of Different Carbon Nanotubes on the Mechanical Properties of Epoxy Matrix Composites − A Comparative Study. *Compos. Sci. Technol.* **2005**, *65* (15), 2300−2313.
(52) Rafiee, M. A.; Rafiee, J.; Wang, Z.; Song, H.; Yu, Z. Z.; Koratkar, N. Enhanced Mechanical Properties of Nanocomposites at Low Graphene Content. *ACS Nano* **2009**, *3* (12), 3884−3890.
(53) Bortz, D. R.; Heras, E. G.; Martin-Gullon, I. Impressive Fatigue Life and Fracture Toughness Improvements in Graphene Oxide/Epoxy Composites. *Macromolecules* **2012**, *45* (1), 238−245.
(54) Lee, C.; Wei, X.; Kysar, J. W.; Hone, J. Measurement of the Elastic Properties and Intrinsic Strength of Monolayer Graphene. *Science* **2008**, *321* (5887), 385−388.
(55) Ma, P. C.; Kim, J. K. *Carbon Nanotubes for Polymer Reinforcement*; CRC Press and Taylor & Francis: Singapore, 2011.
(56) Wang, X.; Jin, J.; Song, M. An Investigation of the Mechanism of Graphene Toughening Epoxy. *Carbon* **2013**, *65*, 324−333.
(57) Chandrasekaran, S.; Sato, N.; Tölle, F.; Mülhaupt, R.; Fiedler, B.; Schulte, K. Fracture Toughness and Failure Mechanism of Graphene Based Epoxy Composites. *Compos. Sci. Technol.* **2014**, *97*, 90−99.
(58) Leguillon, D.; Piat, R. Fracture of Porous Materials − Influence of the Pore Size. *Eng. Fract. Mech.* **2008**, *75* (7), 1840−1853.
(59) Deng, Z.-Y.; She, J.; Inagaki, Y.; Yang, J.-F.; Ohji, T.; Tanaka, Y. Reinforcement by Crack-Tip Blunting in Porous Ceramics. *J. Eur. Ceram. Soc.* **2004**, *24* (7), 2055−2059.

DOI: 10.1021/acsami.5b06476
ACS Appl. Mater. Interfaces 2015, 7, 21455−21464